Assessing Hydraulic Fracturing in Earthen-Rockfill Dam Core based on Extended Finite Element (XFEM) Framework

Anulekha Chakraborty
Research Scholar, Department of Civil Engineering, Indian Institute of Technology Guwahati, Assam, India; Email: canulekha@iitg.ac.in

Arindam Dey* (Corresponding author)
Associate Professor, Department of Civil Engineering, Indian Institute of Technology Guwahati, Assam, India; Email: arindam.dey@iitg.ac.in

Sachin Singh Gautam
Associate Professor, Department of Mechanical Engineering, Indian Institute of Technology Guwahati, Assam, India; Email: ssg@iitg.ac.in

Abstract

Hydraulic fracturing in clay core of earth-rock fill dams appear when fluid pressure becomes higher than the total stress at a point, developing tensile effective stress conditions within the soil. In this paper, hydraulic fracture in an earth-rockfill dam is modelled using eXtended Finite Element Method (XFEM). The finite element simulation of Hyttejuvet dam is carried out to exhibit the pore pressure developments at various locations of the dam, which are compared with measured in-situ measurement and monitoring data. A prominent arching at the mid-depth of the upstream core face could be noticed at the location of crack appearance in the dam. The fracture occurs in a nearly vertical direction, orthogonal to the maximum effective tensile stress direction within the core. The influence of various characteristic properties of core material on initiation of hydraulic fracture is investigated. It is concluded that increasing the permeability of the core delays the fracture initiation while inducing a smaller crack in the core. Adopting a core material with higher modulus of elasticity can reduce arching phenomenon in the dam to ensure a less severe crack formation. Additionally, increase in the maximum reservoir level is found to induce larger crack in the dam core.

Keywords: eXtended Finite Element Method, Hydraulic fracturing, Earth-rockfill dam, Effective stress principle, Arching.

1. Introduction

Several types of dams, such as the arch dam, gravity dam, arch-gravity dam, barrage and embankment dams are built for the purpose of water storage, barrier, hydropower generation and irrigation (Angelakis *et al*., 2024). However, with approximately 72-77% of all the varieties of dams around the world, embankment dams constitute the major share (Wiltshire, 2002; Adamo *et al*., 2020). Typically constructed from compacted earth, these dams rely on their mass to counteract the pressure exerted by water, which is, in a way, similar to gravity dams made out of concrete. An embankment dam consisting of free draining granular earth (like gravels and rock fills) with an impervious soil core is termed as 'Composite dam' or an 'Earth-rockfill dam' (Wang, 2014). Despite their prevalence, embankment dams carry a heightened risk of failure, as they are more sensitive to hydraulic problems compared to concrete dams due to the inherent characteristics of their construction materials (Wang, 2014; Adamo *et al*., 2020; Talukdar and Dey, 2019). Cracks are a common occurrence in the soil core of earth-rockfill dams, often attributed to the stress arching action due to differential settlements between the core and shell or hydraulic fracturing from the seeping water (Zhu and Wang, 2004; Talukdar and Dey, 2021).

Instances of dam failures or damage caused by concentrated leaks have been extensively documented (USCOLD, 1988; ICOLD, 1995). In some cases, even in the absence of visible surface cracks, investigators have attributed these incidents to probable causes such as differential settlement cracks (Sherard, 1986). Notably, in several instances, concentrated leaks emerged abruptly on the downstream side of dams after first reservoir filling, suggesting that significant open cracks were absent beforehand (Binnie, 1978; Binnie, 1983; Kjærnsli and Torblaa, 1968). This highlights the potential of reservoir water pressure to either induce the opening of existing closed cracks or create new ones under specific conditions. Hydraulic fracturing is a phenomenon where the water pressure, due to impounding, induces or widens cracks in rock or soils, and the same is well-documented. It is often described as a phenomenon where fracturing occurs in the least resistant soil under increased water pressure (Jaworski *et al*., 1981). Even though hydraulic fracturing can occur in homogenous embankments, it is more likely to be exhibited in dams with varying materials having different deformability and permeability (Sherard, 1973). Due to the low permeability of the core material, as water wedging action occurs in the cracks (Djarwadi *et al*., 2017), the phenomenon of hydraulic fracturing remains to be particularly damaging the soil core of earth-rock fill dams. Despite

significant attention is drawn to his particular aspect of hydraulic fracturing since the Teton Dam failure in 1976 (USBR, 1976), the challenge of hydraulic fracturing still remains largely unsolved and comprise a challenging field of research.

Prior to 1976, few studies acknowledged that hydraulic fracturing could lead to concentrated leaks, resulting in further damage or erosion of dams (Kjærnsli and Torblaa, 1968). There are limited field studies published on hydraulic fracturing in embankment dams (Kjærnsli and Torblaa, 1968; Vaughan *et al*., 1970; Vestad, 1976; Penman and Charles, 1981; Sherard, 1986). Kjærnsli and Torblaa (1968) concluded that the sudden excessive leakage in Hyttejuvet dam in Norway was caused by arching of the core followed by hydraulic fracturing when the reservoir filling took place. Lofquist (1951) was among the first to discuss the presence and implications of arching in rockfill dams, emphasizing the cause of stress reduction due to differential settlement of the dam core. Sherard (1986) concluded that concentrated leaks often arise through the impermeable sections of embankment dams due to hydraulic fracturing, even in those dams that remain unaffected by significant differential settlement. Hydraulic fracture in many earthen dams have been documented and studied, which includes the Hyttejuvet Dam by Kjaernsli and Torblaa (1968), the Teton Dam by Seed and Duncan (1981), and various old British dams by Dounias *et al*. (1996). After the Teton dam failure in 1976, there has been a resurgence of interest among researchers, leading to numerous publications exploring various aspects of concentrated leak development through hydraulic fracturing (Dascal, 1984; Jaworski *et al*., 1981; Seed and Duncan, 1981).

Numerical simulation methods were widely used to investigate hydraulic fracturing. Ng and Small (1999) studied the development of hydraulic fracturing using finite element method, allowing the simulation of complete history of pore pressure development in the core of the dam. Special joint elements, which cracks open when effective stress in the element reduces to zero (Ng and Small, 1997), were used to model the fracturing. Li *et al*. (2007) applied the smeared cracking theory to model hydraulic fracturing in an earth and rockfill dams. Cohesive fracture model that requires mesh updating at the crack tip during successive cracking was used by Secchi and Schrefler (2012). Barani and Khoei (2014) used double-noded zero-thickness cohesive interface elements to model the fracture behaviour in saturated porous medium. Ji *et al*. (2018) used extended finite element method (XFEM) to simulate hydraulic fracturing behaviour in an earth-rockfill dam. The authors had used plane strain elements and defined the hydrostatic pressure in the crack as a facial pressure on the crack surface.

Several hydraulic fracturing criteria have also been developed by various researches based on geomechanics and fracture mechanics. Komak Panah and Yanagisawa (1989) suggested the minimum hydraulic fracture pressure in the shear mode of cracking based on Mohr-Coulomb criterion while the same in the tension mode occurs when the maximum value of effective tensile stress at failure becomes constant and proportional to tensile strength of the material. In the similar line, Lo and Kaniaru (1990) conducted hydraulic fracturing laboratory tests and developed simple theoretical expressions for the fracture pressure based on soil strength parameters. Tresca-, Mises-, or Coulomb- criteria, based on the yield dominant failure, can be used to assess the yield induced failure of materials, but does not help to investigate fracture dominant failure (Chudnovsky *et al*., 1988). Wang *et al*. (2007) provided a hydraulic fracture propagation criterion based on experimental observations and linear elastic fracture mechanics (LEFM). The authors have suggested that hydraulic fracturing in earth-rock fill dams is facilitated by four key conditions: the presence of a crack at the upstream face of the core, the low permeability of the core soil, rapid impoundment of water and the presence of unsaturated soil in the core.

In this study, XFEM-based cohesive segments method in ABAQUS has been used to simulate the hydraulic fracturing of earth-rock fill dam. Firstly, a validation study is presented in regard to the failure of the Hyttejuvet dam in which the simulation results are exhibited to be in good agreement with the on-site observations. Further, several factors affecting the behaviour of hydraulic fracture in earth-rockfill dams has been assessed and illustrated, which include permeability, modulus of elasticity of core and the reservoir water level.

2. Theory and Background

2.1 Effective Stress Principle

Pore pressure plays an important role in geological fracturing cases, be it in large scales, such as in faulting, or at the regional scale, such as in the tensile fracturing in the clay core that is often termed as ‘hydraulic fracturing’. The occurrence of tensile fractures in soils and rocks has long been a less understood phenomenon, given that the stresses within earthen structures and the earth's crust are primarily compressive (Guerriero and Mazzoli, 2021). The development of effective stress principle (ESP) has made it possible to define the fracturing mechanism. However, the simple expression given by Terzaghi (1923) cannot appropriately

explain the phenomenon of tensile fracturing. In its one-dimensional form, Terzaghi's expression is given by

$$\sigma' = \sigma - p, \quad (1)$$

where, σ is the total stress, p is the pore pressure and σ' is the effective stress. In multi-dimensional component form, the principle can be written as

$$\sigma'_{ij} = \sigma_{ij} - \delta_{ij}\, p, \quad (2)$$

where δ_{ij} denotes the Kronecker's delta. The conventional positive sign for compressive stresses is adopted in this formulation.

Over the years, the understanding of ESP has sufficiently advanced as several researchers have proposed different laws for effective stress within the general formulation (in one-dimensional form) of

$$\sigma' = \sigma - \eta\, p, \quad (3)$$

where, η is a parameter that depends on the properties of the porous medium as well as on the magnitudes of σ and p.

Several formulations have been proposed over the time for the coefficient η. Some are summarized below:

$$\sigma' = \sigma - p,\ \eta = 1 \text{ ; (Terzaghi, 1923)}$$

$$\sigma' = \sigma - n\, p \text{ ; (Fillunger, 1936)} \quad (4)$$

$$\sigma' = \sigma - (1 - a_c)\, p \text{ ; (Skempton, 1960)} \quad (5)$$

$$\sigma' = \sigma - \left(1 - \frac{K}{K_s}\right) p \text{ ; (Nur and Byerlee, 1971)} \quad (6)$$

where, n is the porosity, a_c is the contact area ratio (contact area between the particles per unit gross area of the material), while K and K_s are the bulk moduli of the porous rock and solid rock, respectively. Researchers have agreed that the fracturing mechanism is possible if the effective stress is defined by the formulation of Equation 3. By this formulation, the fluid pressure in the tensile zone can be higher than the total stress, thereby leading to the development of tensile effective stress in the soil.

2.2 Coupled Pore Fluid and Deformation Analysis in ABAQUS

In ABAQUS/Standard, a porous medium such as soil or rock, is modelled as a multiphase material that implements a general nonlinear unsaturated soil mechanics framework formulated for a three-phase mixture consisting of solid grains, a wetting fluid, and air. The overall material

deforms in response to the saturation-dependent effective stress principle, which was initially introduced by Bishop (1959) for unsaturated soils.

The total stress acting at a point, σ, is assumed to be made of the wetting liquid pressure, u_w, and pressure in the other fluid, u_a (or the interstitial air pressure) and an effective stress, σ', defined by

$$\sigma' = \sigma + [\chi u_w + (1 - \chi)u_a] I . \quad (7)$$

Positive stress components are tensile in nature as per the sign convention in ABAQUS. This explains the sign of the Equation 7. The parameter χ depends on saturation as well as surface tension of the liquid/solid system. If the medium is fully saturated, then χ takes a value of 1.0 and if it is partially saturated, the value is considered between 0.0 and 1.0, depending on the degree of saturation of the system.

An essential element of a poromechanical governing framework is the hydro-mechanical interaction (i.e., coupling) between the fluid and solid constituents. It is governed by the equilibrium equations for porous media and the continuity equation that directs the flow of the wetting liquid. In ABAQUS, a continuity equation for the wetting phase fluid is formulated by equating the rate of change in liquid mass within a control volume to the liquid mass across the associated control surface. The continuity statement is written in variational form as a basis for finite element approximation. Here, the excess wetting liquid pressure is the nodal variable (with 8 degrees of freedom). A control volume containing fixed amount of solid is considered. In the initial configuration, the volume occupies space V with surface S. In the reference configuration, it occupies the volume V^0. Let V_w be the volume of the wetting liquid flowing through the space V at any instant of time. Here, a case of full wetting phase saturation (i.e. no air) and no fluid entrapment to solid particles are considered, thereby making it a two-phase fully saturated poromechanics formulation.

The total mass of wetting liquid in the control volume is given by

$$\int_V \rho_w dV_w = \int_V \rho_w n_w dV , \quad (8)$$

where, ρ_w is the mass density of liquid, n_w is the volume ratio of free wetting liquid at a point. The time rate of change of the wetting liquid mass is given by

$$\frac{d}{dt}\left(\int_V \rho_w n_w dV\right) = \int_V \frac{1}{J}\frac{d}{dt}(J\,\rho_w n_w)dV\,, \tag{9}$$

where, J is the Jacobian. The mass of wetting liquid crossing the surface and entering the volume per unit time is expressed as

$$-\int_S \rho_w n_w \mathbf{n}\,.\,\overline{\mathbf{v}}_w dS, \tag{10}$$

where, $\overline{\mathbf{v}}_w$ is the seepage velocity and $\mathbf{n}$ is the outward normal to the surface S.

Equating the mass of liquid added across surface S to the rate of change of liquid mass within volume V gives the wetting liquid mass continuity equation as

$$\int_V \frac{1}{J}\frac{d}{dt}(J\,\rho_w n_w)dV = -\int_S \rho_w n_w \mathbf{n}\cdot\overline{\mathbf{v}}_w dS, \tag{11}$$

Using Gauss divergence theorem on the RHS and equating the integrand to zero, the following expression is obtained

$$\frac{1}{J}\frac{d}{dt}(J\,\rho_w n_w) + \frac{\partial}{\partial \mathbf{x}}\cdot(\rho_w n_w \overline{\mathbf{v}}_w) = 0, \tag{12}$$

The equivalent weak form is given by

$$\int_V \delta u_w \frac{1}{J}\frac{d}{dt}(J\,\rho_w n_w)dV + \int_V \delta u_w \frac{\partial}{\partial \mathbf{x}}\cdot(\rho_w n_w \overline{\mathbf{v}}_w)dV = 0, \tag{13}$$

where, δu_w is an arbitrary variational field.

Force equilibrium is formulated in the weak form following the principle of virtual work over the same control volume V at time t, which is given as

$$\int_V \boldsymbol{\sigma} : \delta\varepsilon dV = \int_S \boldsymbol{t}\cdot\delta\mathbf{v}dS + \int_V \vec{\mathbf{f}}\cdot\delta\mathbf{v}dV, \tag{14}$$

where, $\delta\mathbf{v}$ is the virtual solid particle velocity, $\boldsymbol{t}$ is the traction on the current control surface, $\delta\varepsilon$ is the virtual rate of deformation, $\boldsymbol{\sigma}$ is the Cauchy stress and $\vec{\mathbf{f}}$ is the body force per unit volume. The body force $\vec{\mathbf{f}}$ will also include the part due to the weight of wetting liquid ($\mathbf{f}_w$) that is expressed as.

$$\mathbf{f}_w = \rho_w n_w \mathbf{g}, \tag{15}$$

Thus, the force balance equation reads

$$\int_V \boldsymbol{\sigma} : \delta\varepsilon dV = \int_S \boldsymbol{t}\cdot\delta\mathbf{v}dS + \int_V \mathbf{f}_b\cdot\delta\mathbf{v}dV + \int_V \rho_w n_w \mathbf{g}\cdot\delta\mathbf{v}dV, \tag{16}$$

where, $\mathbf{f}_b$ are all body forces excluding the weight of the wetting liquid. The equilibrium equations along with the continuity equation collectively establish the condition of the porous medium.

The continuity equation (i.e. Equation 13) and the governing equation (i.e. Equation 16) are coupled equations. To solve these equations, two approaches exist. In the first approach, also termed as the 'staggered approach', one set of equation (say, Equation 16) is solved first assuming the pore pressure as constant. Then, the solution from the first set of equations is used to solve the second set equations (i.e., Equation 13). The results obtained are again used to solve back Equation 16, and the process is iterated until negligible change in the solution is obtained. However, this approach may be time consuming and slow to converge. In the second approach, which is used by ABAQUS/Standard, both the equations (i.e. Equations 13 and 16) are solved simultaneously. This approach is faster as it has better convergence. For more details, the reader is referred to the ABAQUS documentation (SIMULIA User Assistance, 2017).

2.3 XFEM and its Implementation in ABAQUS

Analysing crack propagation remains a significant challenge in the numerical modeling scenarios. This challenge arises because the conventional Finite Element Method (FEM) discretization needs to accommodate the discontinuity. For evolving discontinuities, this necessitates regenerating the mesh at each time step. Consequently, the solution must be re-projected onto the updated mesh at each time step, leading to a substantial increase in computational cost and a reduction in rate of convergence. Due to these limitations, numerous numerical approaches have emerged in recent years to address fracture mechanics problems. To mitigate the need for remeshing, various techniques have been introduced over the last few decades. These include incorporating a discontinuous node at the element level (Oliver, 1995), utilizing a moving mesh technique (Rashid, 1998), or employing an enrichment technique based on the partition of unity (i.e. the sum of the shape functions must be unity) that is termed as the 'eXtended Finite Element Method' or XFEM, as proposed by Belytschko and Black (1999).

XFEM eliminates the need to regenerate the mesh conforming to geometric discontinuities. As an extension of the FEM and based on the concept of partition of unity (Melenk and Babusska, 1996), the standard finite element displacement approximation is enhanced by means of adding enrichment functions. The discontinuities are modelled using special enrichment functions along with additional degrees of freedom. However, this enhancement comes at the cost of increased nodal degrees of freedom. Hence, in XFEM, enrichment is employed only at the local level i.e., elemental nodes close to the crack tip, as well as the ones required for the correct localisation of the crack. It is a very attractive and effective way to simulate initiation and

propagation of a discrete crack along an arbitrary solution-dependent path without the requirement of remeshing in the bulk materials.

The enrichment functions consist of a discontinuous 'jump function' that represents the jump in displacement across the crack surfaces and the 'crack-tip functions' that can capture the singularity around the crack tip. The following expression provides the XFEM approximation of a displacement vector function $\boldsymbol{u}$, and is formulated as

$$\boldsymbol{u} = \boldsymbol{u}_{FEM} + \boldsymbol{u}_{ENR} = \sum_{I\in N} N_I\,(\mathrm{x}) \left[\boldsymbol{u}_I \; + \underbrace{H(\mathrm{x})\boldsymbol{a}_I}_{I\in N_\Gamma} \; + \underbrace{\sum_{\alpha=1}^{4} F_\alpha(\mathrm{x})\boldsymbol{b}_I^{\alpha}}_{I\in N_\Lambda} \right], \qquad (17)$$

where, $\boldsymbol{u}_{FEM}$ denotes the usual FEM approximation and $\boldsymbol{u}_{ENR}$ is the additional enrichment. $N_I\,(\mathrm{x})$ are usual nodal shape functions, $\boldsymbol{u}_I$ is the nodal displacement vector for all the nodes in the model, $\boldsymbol{a}_I$is the nodal enriched degree of freedom vector for elements completely cut by the crack. Here, $H(\mathrm{x})$ is the discontinuous jump function or the Heaviside function, employed to the enriched elements completely cut by the crack. The splitting of the domain by the crack causes a jump in the displacement field, for which the Heaviside function provides a simplistic mathematical tool to represent such phenomenon. In Equation (17), N_Γ represents the nodes belonging to elements cut by crack and N_Λ represents nodes belonging to elements containing crack tip, $\boldsymbol{b}_I^{\alpha}$ is the nodal enriched degree of freedom vector for the elements containing crack tip, and $F_\alpha(\mathrm{x})$ are the crack tip functions that represent the crack tip singularity. In case of that elements that are not completely cracked, the Heaviside function cannot be used to approximate the displacement field over the entire element domain, since the element contains the crack tip. The Heaviside and the crack tip enrichment functions are multiplied by the conventional shape functions.

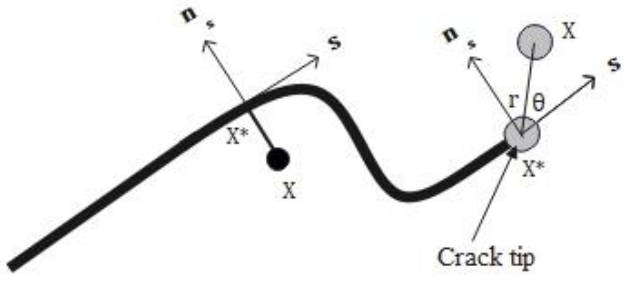

Figure 1. Normal and Tangential coordinates for a smooth curve used in crack-tip function

The discontinuous jump function across the crack surfaces, $H(\mathrm{x})$, given by

$$H(\mathrm{x}) = \begin{cases} 1 & \text{if } (\mathbf{x} - \mathbf{x}^*).\mathbf{n_s} \geq 0, \\ -1 & \text{otherwise,} \end{cases} \tag{18}$$

where, $\mathbf{x}$ represents the location of Gauss point, $\mathbf{x}^*$ is the point on the crack closest to $\mathbf{x}$, and $\mathbf{n_s}$ is the unit normal to $\mathbf{x}^*$.

For an isotropic elastic material, the crack tip functions, as illustrated in Figure 1, can be defined as

$$F_\alpha(x)_{\alpha=1}^4 = \left\{\sqrt{r}\cos\left(\frac{\theta}{2}\right), \sqrt{r}\sin\left(\frac{\theta}{2}\right), \sqrt{r}\sin\left(\frac{\theta}{2}\right)\sin(\theta), \sqrt{r}\cos\left(\frac{\theta}{2}\right)\sin(\theta)\right\}, \tag{19}$$

where, (r, θ) is a polar coordinate system with origin at the crack tip and $\theta = 0$ is tangent to the crack tip. More details on crack tip functions are discussed in Sukumar *et al.* (2004).

In ABAQUS/Standard, the implementation of XFEM relies on the phantom nodes method (Figure 2). In this method, phantom nodes remain tied to their corresponding standard nodes at the steps when the enriched element remains intact. However, when a crack initiates and the element is cut by the crack, it splits into two separate parts. Each part includes both real and phantom nodes to accurately model the behaviour of the crack within the element.

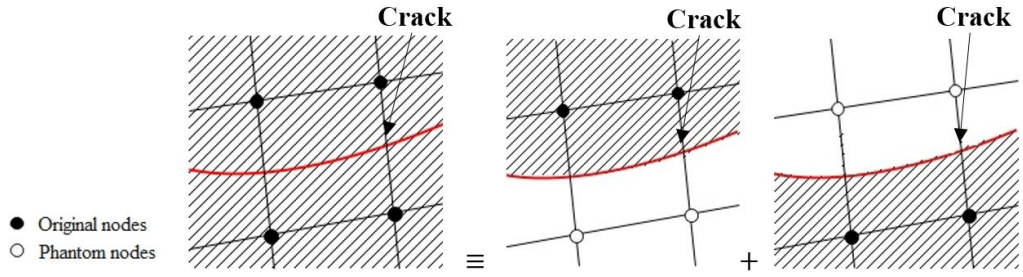

Figure 2. Phantom nodes method for the implementation of XFEM in ABAQUS/Standard

In ABAQUS, two types of damage modelling within the XFEM framework is available. First is the XFEM based cohesive segments approach, which is used in the present study. The second is the linear elastic fracture mechanics (LEFM) approach. In XFEM based cohesive segment approach, damage modelling is achieved through the use of traction-separation law for damage initiation and evolution. The process identifies critical regions of crack initiation where stress or strain exceeds the user defined critical value, after which the phantom nodes detach from the superposed original real nodes. For the prediction of damage initiation, the maximum

principal stress damage criterion is used. It assumes that a crack will nucleate as soon as the stress ratio (R) reaches a value equal to 1, which is expressed as

$$R = \left\{ \frac{\langle \sigma_{max} \rangle}{\sigma_{max}^{o}} \right\}, \tag{20}$$

Here, σ_{max}^{o} represents the maximum allowable principal stress, while the symbol $\langle\ \rangle$ indicates the Macaulay brackets, used to signify that a purely compressive stress state does not lead to any damage initiation. Such criteria define the conditions at which an internal defect will nucleate within the body. Next, the evolution of damage is defined by two main components. The first component entails defining either the effective displacement at complete failure, δ_m^f, relative to the initial effective displacement at the onset of damage, δ_m^o, or quantifying the energy dissipated during failure, G^C. The second aspect of defining damage evolution involves determining how the damage progresses between initiation of failure at point A and final failure point B (Figure 3). This can be achieved by establishing linear or exponential softening laws, or directly specifying damage variable, D as a function (in a tabular format) relative to the effective displacement at the initiation of damage. Damage variable represents the amount of deterioration due to crack growth. A simple energy based linear softening model is used as the damage evolution model in the present study. Linear softening specifies a linear softening stress–strain response for linear elastic materials or a linear evolution of the damage variable with deformation for elastic–plastic materials.

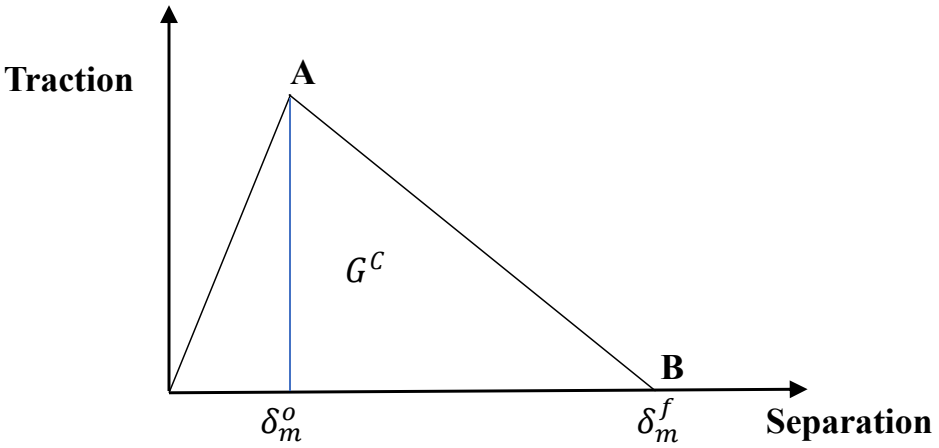

Figure 3. Typical traction-separation response with a linear softening damage evolution

In ABAQUS, the cohesive segments, along with phantom nodes approach, of XFEM is extended to model fractures driven by hydraulic pressures. Phantom nodes having pore-pressure degrees-of-freedom are present on the edges of enriched element to model fluid flow

within the crack surface along with phantom nodes that represent the displacement discontinuities and fluid pressure in a cracked element. By performing a coupled pore fluid diffusion and stress analysis, the fluid pressure on the surfaces of the crack elements influences the traction-separation behaviour of the cohesive segments within the enriched elements.

3. Hydraulic Fracturing of Hyttejuvet Dam

Hyttejuvet dam is one of the most studied cases of hydraulic fracturing in earthen dams (Kjærnsli and Torblaa, 1968; Ng and Small, 1999; Li *et al*., 2007; Haeri and Faghihi, 2008). It is an earth and rockfill dam located in Norway, having a height of 93 m and 400 m crest length. The dam was built between 1964 and 1965. The dam has a narrow and nearly vertical core, consisting of well-graded moraine, and the shells that are mainly constructed of gravel and rocks. The construction of the entire embankment took around 520 days and was completed in two construction seasons (as shown in Figure 4). Following the initial construction season in 1964, it was observed that the pore-water pressures measured onsite exceeded the expectations. Consequently, the design underwent revisions to facilitate quicker dissipation of pore-water pressures from within the core. This led to a reduction in the core width at the upper section of the dam in the subsequent construction season. This adjustment is highlighted by a noticeable reduction in core thickness at the elevation of 700 meters, as depicted in Figure 5. First filling of the reservoir was started from May 1966. An unexpected severe leakage occurred during the first impounding of the reservoir, when the reservoir level was about 7 m below the regulated water level. Figure 6 shows the first reservoir filling and leakage data observed with respect to time. The x-axis marker indicates months, where J denotes January and so on. As the leakage increased suddenly when the water level rose to 738 m, it was required to reduce the rate at which the reservoir filling was taking place. Afterwards, several boreholes were sunk and percolation tests were done to investigate the leakage. During these tests, water in the reservoir was filled at a slower rate and the consequent leakage was observed to be lessened. Kjærnsli and Torblaa (1968) concluded that the leakage was caused by arching of the core followed by hydraulic fracturing when the reservoir filling took place. This dam has been chosen for the present study because of the availability of measured field data. In order to measure the performance of the dam at various stages, pressure cells were installed in the core to monitor the pore water pressure and earth pressure development. Settlement bolts were positioned along the crest of the dam and on the upstream slope. Additionally, an overflow weir was built downstream to the dam to gauge the seepage through the dam upon reservoir filling.

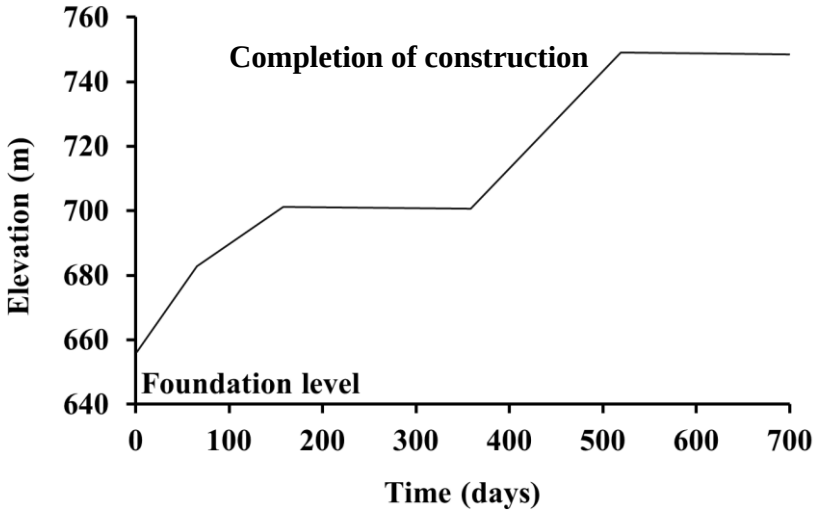

Figure 4. Construction stages of Hyttejuvet dam height with respect to time

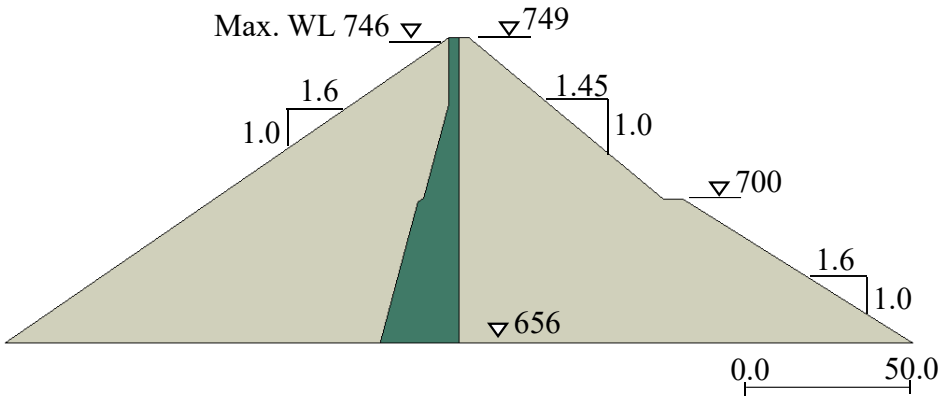

Figure 5. Typical section of Hyttejuvet dam exhibiting thinner core width in the upper section of the dam during its second construction season

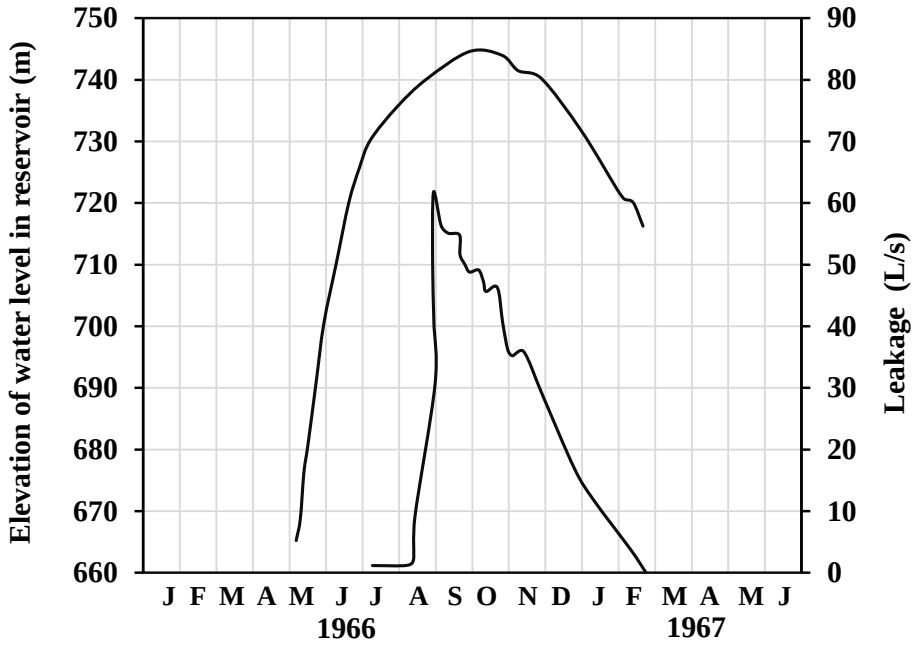

Figure 6. Elevation of water level and leakage record during first filling of reservoir

4. Numerical Modelling of the Hyttejuvet Dam

In this paper, coupled pore fluid diffusion and stress based finite element analysis is adopted to study the onset of hydraulic fracturing in Hyttejuvet dam using ABAQUS 2017. This allows to study the development of transient pore water pressures and deformations within the dam. In this method, in ABAQUS, a porous medium is treated as a multiphase material and employs an improvised version of effective stress principle to characterize its behaviour. Cracking in the dam is modelled by using the XFEM provision in ABAQUS, as has been discussed earlier. The schematic layout of the dam section is shown in Figure 5. CPE4P (4 noded plane strain quadrilateral, bilinear displacement and pore pressure) elements are used to discretise the dam. Construction of the embankment is carried out in stages, as per the construction time line shown in Figure 4, using the 'model change' feature in 'interaction' module of ABAQUS. The gravity loading of the layers is applied gradually in 4 steps. After the completion of construction, 177 days of consolidation period is allowed before the commencing the filling of the reservoir. Filling of the reservoir, until maximum elevation of 745 m, is carried out in approximately six months using transient 'Soils' step. The reservoir water is simulated by assigning pore pressure boundary condition, equal to the total head at a given point, along the immersed part of the upstream slope of the dam. Displacement on the bottom boundary of the dam is restricted in all directions. The downstream slope is defined as a freely draining surface by prescribing

373 *FLOW keyword in ABAQUS, which prescribes flow velocity on the surface in a way that
374 approximately renders zero pore pressure on the saturated portion of this surface.
375 The moraine material used to construct the core of the dam is modelled using elastic-modified
376 Drucker Prager / Cap plasticity constitutive model. The gravel and rockfill shells were assumed
377 to be elastic. Table 1 list the properties of the materials used for the analysis, which are adopted
378 from available standard literatures on Hyttejuvet dam (Kjærnsli and Torblaa, 1968; Ng and
379 Small, 1999; Haeri and Faghihi, 2008).
380
381 **Table 1.** Material properties used in the numerical modelling of the Hyttejuvet dam

Shell		Core	
Young's Modulus, E	50000 kPa	Material Cohesion, d	51.24 kPa
Poisson's ratio, v	0.3	Angle of friction, β	44.9°
Void ratio, e	0.5	Cap eccentricity, R	1
Permeability, k	0.0225 m/s	Initial cap position	0
Unit weight, γ	22.00 kN/m^3	Transition surface parameter, α	0.01
		Flow stress ratio, K	0.8
		λ	0.035
		κ	0.0015
		Poisson's ratio, v	0.3
		Void ratio, e	0.26
		Permeability, k	7×10^{-10} m/s
		Unit weight, γ	22.66 kN/m^3

382
383 The response of cohesive traction-separation behaviour of the core is specified. The maximum
384 principal stress damage criterion is selected for damage initiation, and energy-based damage
385 evolution law is selected for damage propagation. The fracture energy and maximum principal
386 stress taken are 7.05 N/m and 20 kPa, respectively, from a typical tensile load-displacement
387 curve of soil specimens provided by Tang *et al*. (2015). The researchers developed a direct
388 tensile test apparatus to determine tensile strength of compacted clayey soil over a broad range
389 of dry densities and compaction water content. Assuming that tensile strength of clay is very
390 small, in this study, 20 kPa was assumed as the tensile strength of the core clay. Wang *et al*.
391 (2007) also reported that the tensile strength of a clay, which was used as the core material of
392 a high earth-rock fill dam in Western China, varied from 19 kPa to 90 kPa with varying water
393 contents and dry densities of the soil columns. Hence, the assumption for the current study is
394 reasonable. ABAQUS uses sorption curve i.e. the relationship between degree of saturation

(S_r) and negative pore pressure ($-U_w$) for defining the unsaturated behaviour of constituent soil. For any region that is subjected to positive pore pressures, the degree of saturation is considered as S_r =1.0. The sorption curve of the dam materials, as adopted from Haeri and Faghihi (2008), is illustrated in Figure 7. The shells of the dam are highly permeable and no pore water pressures would build up in the shells during construction of embankment stage i.e. before the filling of the reservoirs. Hence, in order to maintain the saturation of the shells as it is in the beginning of the construction, a constant value of pore pressure as per the sorption curve of the shell was considered in the initial stages before the reservoir impounding commenced. By default, in ABAQUS, the permeability of the unsaturated parts of the dam is defined such that it varies as cubic function of degree of saturation.

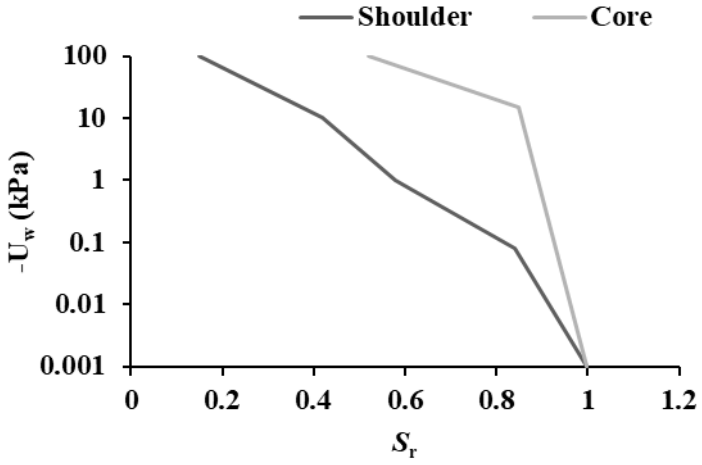

Figure 7. Sorption curve of the dam materials as used in the present study

5. Results and Discussions

5.1 Validation of the Numerical Model of Hyttejuvet Dam

The performance of the developed numerical model of the Hyttejuvet dam is first validated with the parameters measured and monitored in the field. Pore-water pressure measurements at various locations in the core of the dam, as marked in Figure 8, is obtained from Kjærnsli and Torblaa (1968), and the same are used for benchmarking and comparison with the computed values obtained from the present study. Figure 9 shows the comparison of the temporal variation of the pore-water pressure at each of the monitoring points. An appreciable agreement may be noted in the trend and magnitudes of the field-measured values with the ones obtained from the numerical simulation. Minor deviations (marginally lower magnitude of simulated results) in the comparatives can be observed which is quite possible in accordance

to the changes in compaction state which might not always be uniform in the field and which cannot be exactly replicated in the numerical model. The simulation results are also verified with the finite element simulation results by Ng and Small (1999). The trend and the magnitudes of pore pressure evolution obtained in the present study during construction and water impounding are closely matching with the literature.

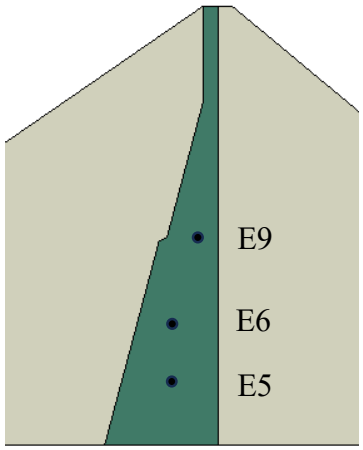

Figure 8. Pore-water pressure monitoring locations selected for comparison with present study (after Kjærnsli and Torblaa, 1968)

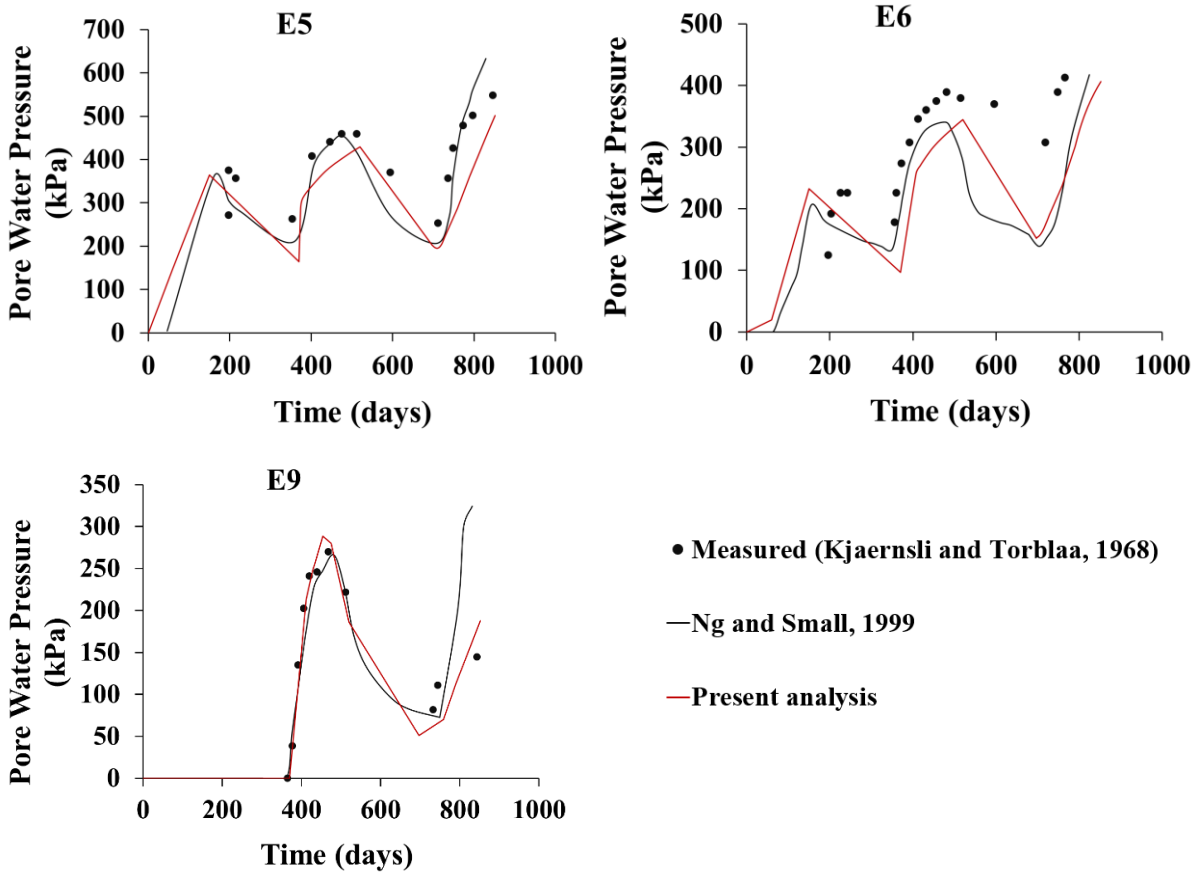

Figure 9. Computed and measured pore-water pressures in the core at monitoring locations (a) E5 (b) E6 (c) E9

5.2 Evolution of Pore-water Pressure during the Construction Stages

Figure 10 depicts the pore pressure development at various stages of the reservoir functioning. The contours show that pore-water pressures build up during construction in the impermeable core (Figures 10a and 10b), while after completion of construction, it gets dissipated in the resting period before impounding starts (Figure 10c). This is quite explainable as a relatively quicker construction process (raising of embankment in lesser time duration) leads to an apparent undrained scenario within the dam body due to an ongoing loading and compaction

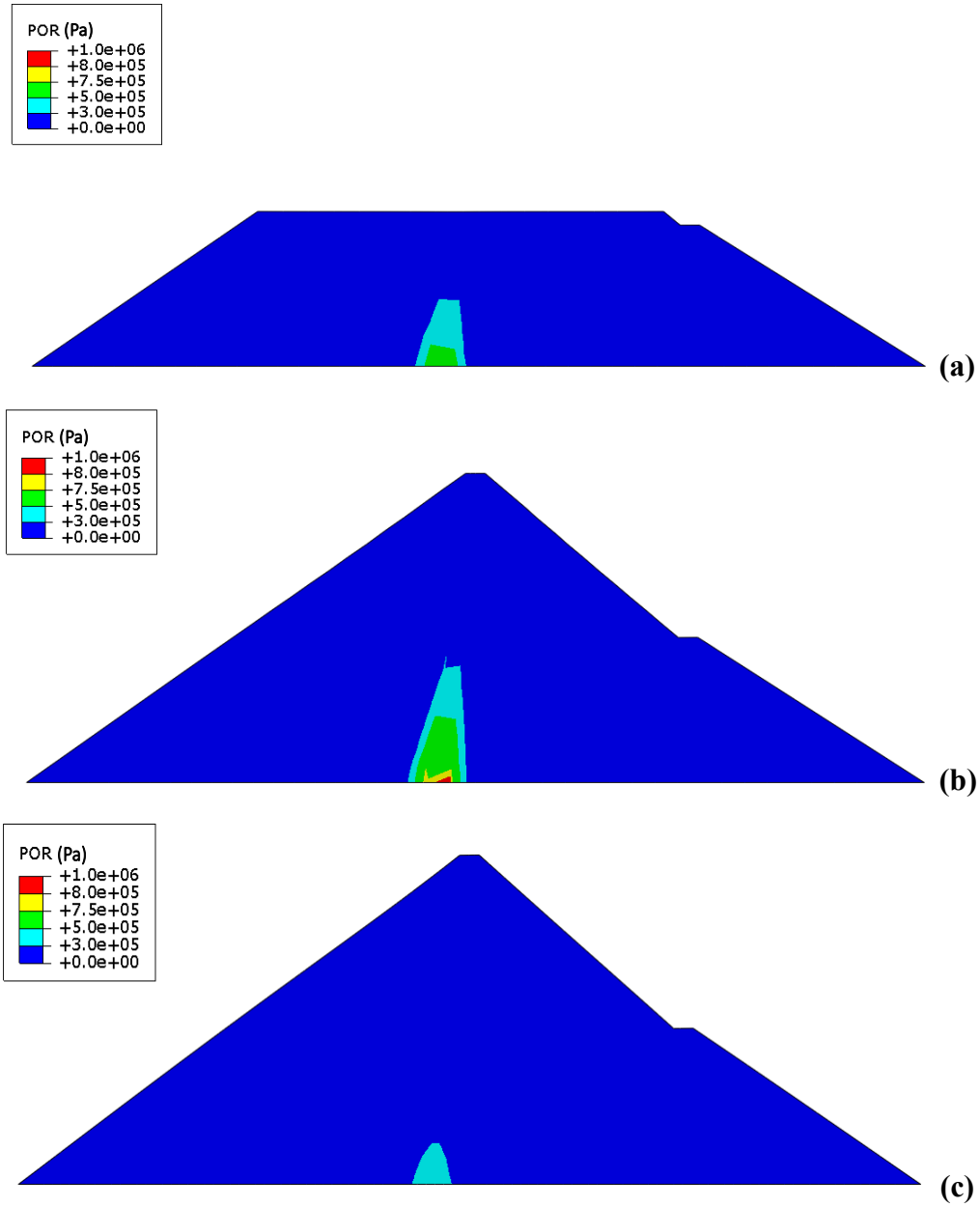

Figure 10. Evolution of pore-water pressure within the dam at various stages of construction (a) during construction at t = 407 days (b) just after completion of construction (c) after resting period of 177 days

process. The rise in pore-water pressure is more pertinent in the constituent materials with lesser permeability, which is the core of the dam in this case. Evidently, with the completion of construction and the rest period allowed, there would be gradual dissipation of the apparent pore-water pressure, and the same is reflected in the Figure 10c. Figure 11 shows the development of pore water pressure as the reservoir is filled. Pore pressure values increase within the embankment due to external hydraulic pressure. Ng and Small (1999) has reported similar observation based in similar finite element simulations of Hyttejuvet dam.

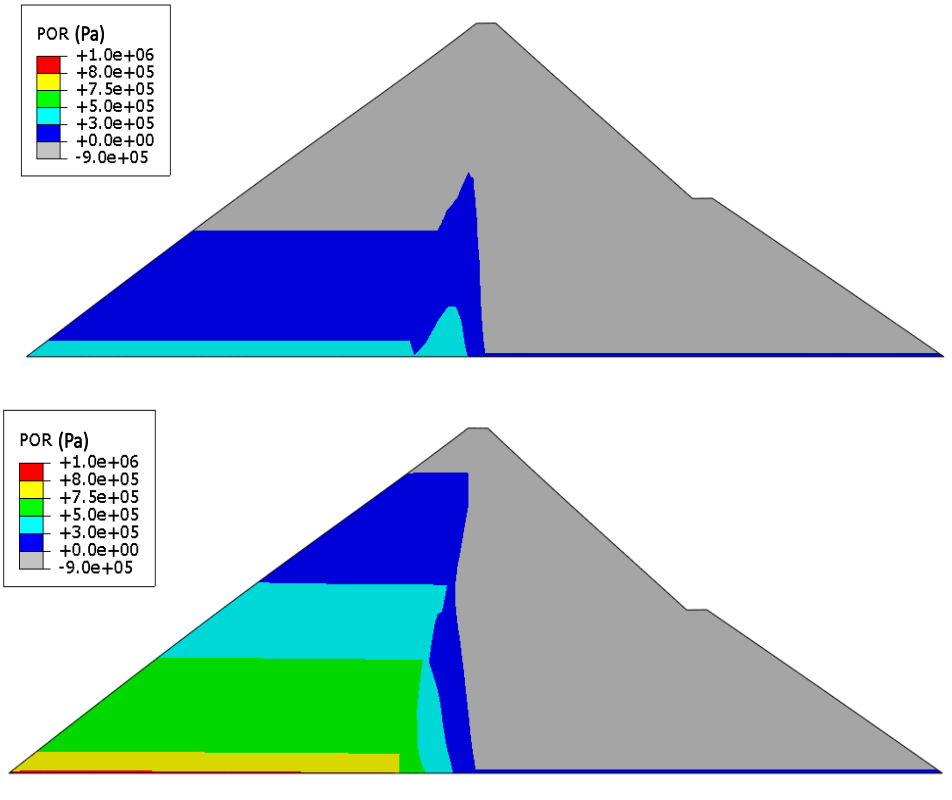

Figure 11. Pore-water pressure development in the dam during reservoir filling (a) when water elevation is at 695 m (b) when water elevation is maximum at 745 m

5.3 Evolution of Differential Settlement and Arching within the Dam Core

Figure 12 shows deformed mesh of the dam during construction of the embankment. After the first season of construction is over, it is observed that the core settles relatively more than the shells, as exhibited in Fig. 12a. Differential settlement continues as the next stages of construction is carried out. Figure 12b shows settlement in the dam after completion of construction. As the stiffness of the clay core is relatively lesser than the shell material, it will tend to deform more as the vertical stresses develop due to the weight of the overburden material, which will eventually lead to the transfer of some vertical stresses from the softer

core to the stiffer shells. This phenomenon, also referred to as 'transverse arching', leads to a decrease in the vertical stresses within the core. This phenomenon eventually hastens hydraulic fracturing in the core as the reservoir filling starts. Kjærnsli and Torblaa (1968) concluded from their field investigation that the cause of leakage in the Hyttejuvet dam was primarily due to arching of the core, which successively led to hydraulic fracturing as the reservoir was filled for the first time

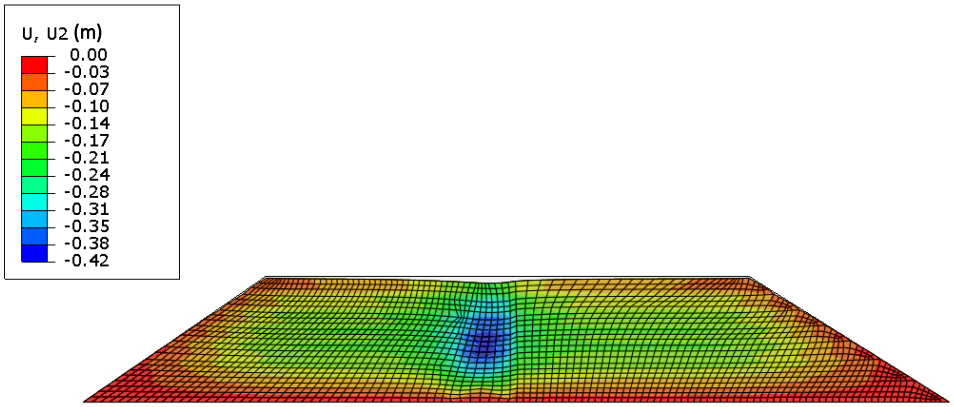

(a)

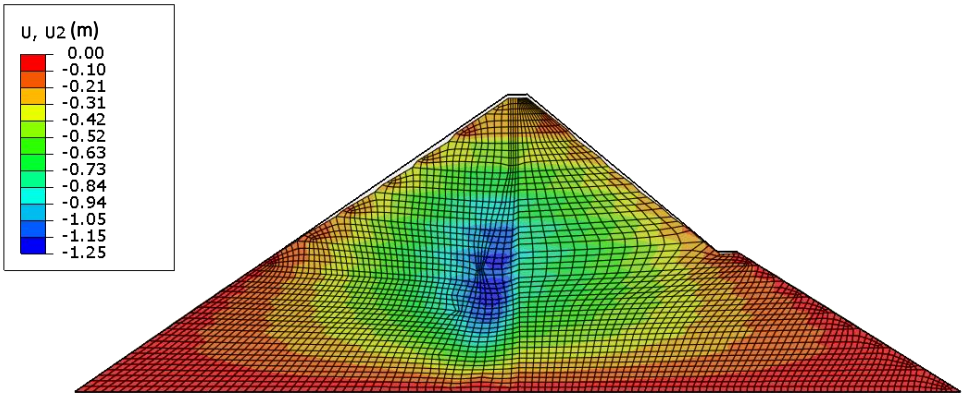

(b)

Figure 12 Deformed mesh and vertical settlement contour (a) after first season of construction (b) after completion of construction of the dam

Figure 13 shows the contour of effective vertical stress developed within the embankment after the construction is completed. As stated earlier, according to sign convention in ABAQUS, negative sign indicates compressive stresses. The vertical stresses in the core are observed to be lesser than the adjacent areas in the shells at same elevation level. Arching in the dam can be quantified by computing the average load transfer ratio or arching factor, R_L, given by

$$\mathrm{R}_L = \frac{\sigma_v}{\gamma h}, \tag{21}$$

where, σ_v is the total vertical stress developed within the dam body and γh gives the stress at a point that should have generated due to overburden height of material (h) above that point considering the deformed geometry. If the value of R_L is less than 1, then arching has occurred in the core. An arching factor close to zero indicates severity of the arching within the dam body. Figure 14 gives the variation of R_L with depth computed for upstream face of the core. It can be seen that arching is more prominent at the mid-depth of the upstream core face where major cracking was predicted by Ng and Small (1999) i.e. 50 m above the dam foundation.

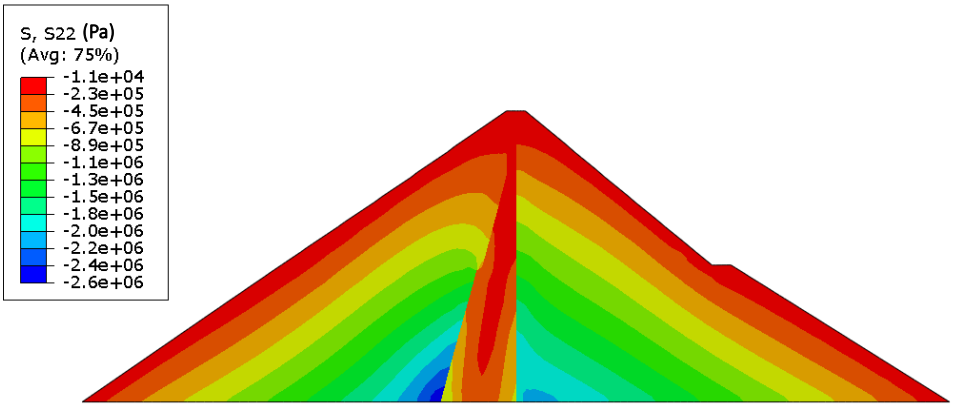

Figure 13. Effective vertical stress contour at the end of construction of dam

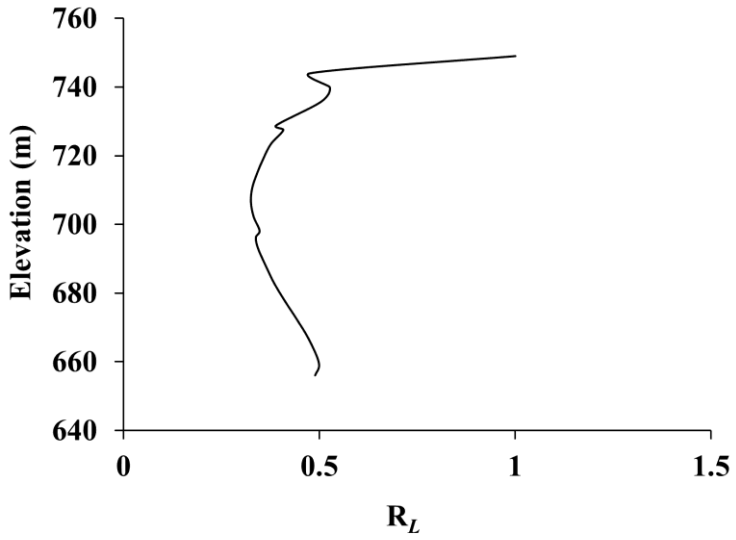

Figure 14. Average load transfer ratio along the upstream face of the core exhibiting the presence of arching in the dam core

Crack appears in the dam core at the locations where prominent arching phenomenon was observed and at locations where the core thickness was drastically reduced during the second

season of construction. Figure 15 reveals the occurrence fracture at the third month of reservoir filling, when the impounding water level was maximum. Figure 16 shows the temporal evolution of the cracking of elements in core during the first filling of reservoir. The reservoir filling is simulated in 6 steps of one month each. The 'step time' shown in Fig. 16 indicates the time completed in each step in seconds. It is observed from the simulation that the fracture initiates approximately at 2.8 months of the first reservoir filling. As shown in Fig. 6, the onsite records portrayed rapid increase in leakage at the downstream weir around at 3.5 months since the commencement of reservoir filling (Kjærnsli and Torblaa, 1968). Considering the delay in time between fracturing and collection of leakage at the downstream weir, the simulated timing of fracturing in this analysis is considered to be reasonably correct.

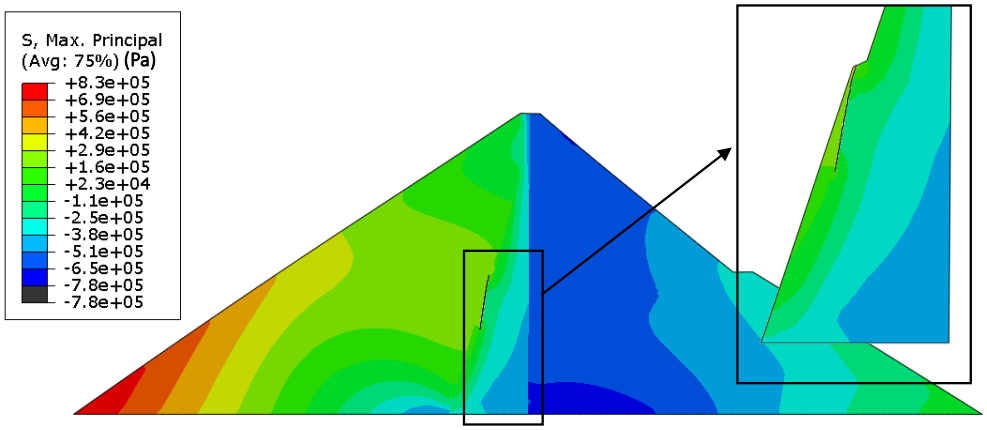

Figure 15. Effective maximum principal stress contour and fracture in the dam core at the sixth month of reservoir filling

This situation of hydraulic fracturing might arise if the total stress in the core is reduced by the arching effect while the pore water pressure increases in the core due to impounding. In such scenario, if the latter becomes higher than the decrease in total stress, tension zone would be created. In this circumstance, the effective stresses in the soil would be estimated following the modified expression (Eq. 3) rather than following the conventional form (given by Eq. 1). Fracturing occurs in the upstream face of the clay core when the tensile effective stresses, rather than the total stress, exceeds tensile strength of the clay. Figure 15 shows that upon seepage of pore water, the effective maximum principal stress becomes positive (i.e. tensile) at the upstream face of the shell until the shell-core interface (light green contour areas). Fractures initiate at the upstream face of core in these tensile zones when the effective maximum principal stress exceeds the tensile strength of the clay. The tensile strength of the rockfill

material in the shell is much higher than clay, thereby no such tension cracks is likely to occur in the shell.

Figure 16 exhibits that the fracture evolves in a nearly vertical direction as the damage initiation criteria is met in the subsequent elements, which is orthogonal to the maximum principal stress or, in this case, the direction of maximum principal stress in tension within the elements. Figure 17 exhibits an exaggerated view of the crack geometry, in which the arrow symbols portray the direction at which maximum principal stress acts in the elements where the crack has initiated. According to maximum principal stress criteria of damage initiation, fracturing occurs orthogonal to the maximum principal stress direction. Hence, in our study, a vertical fracture is obtained, since the effective maximum principal stress in tension would develop in horizontal directions due to pore water pressures developed. This is in contrast to the assumption of Ng and Small (1999), where the researchers have assumed horizontal joint elements to model hydraulic fracturing in the Hyttejuvet dam. On the contrary, based on the cohesive segments approach in this study, the application of XFEM has successfully enabled simulation of the appropriate crack initiation due to hydraulic fracturing and its possible and subsequent path of propagation through the core of the dam.

5.4 Pertinent Factors influencing Hydraulic Fracturing of Zoned Dam

It has been revealed in the previous sections that occurrence of arching within the dam, especially in its core, is a primary factor in initiating cracking within the dam body. Hence, various characteristic parameters of the core material that directly or indirectly influences the stress arching phenomenon would also, in turn, influence the hydraulic fracturing of the dams. In this regard, stiffness of the core material, as well as its permeability, would influence the initiation and occurrence of hydraulic fracturing. From field case-studies, it has been substantiated that the rise in reservoir water level and its rate of filling often controls the leakage and erosion from dams. In this section, the above-stated factors are varied to comprehend their influence on the hydraulic behaviour and fracturing of a dam. For this section of the study, simplified linear elastic material model is considered for both core and shell material, to facilitate ease in varying the parameters at a lesser computational expense. Table 2 lists the material properties as per the different scenarios adopted for this analysis.

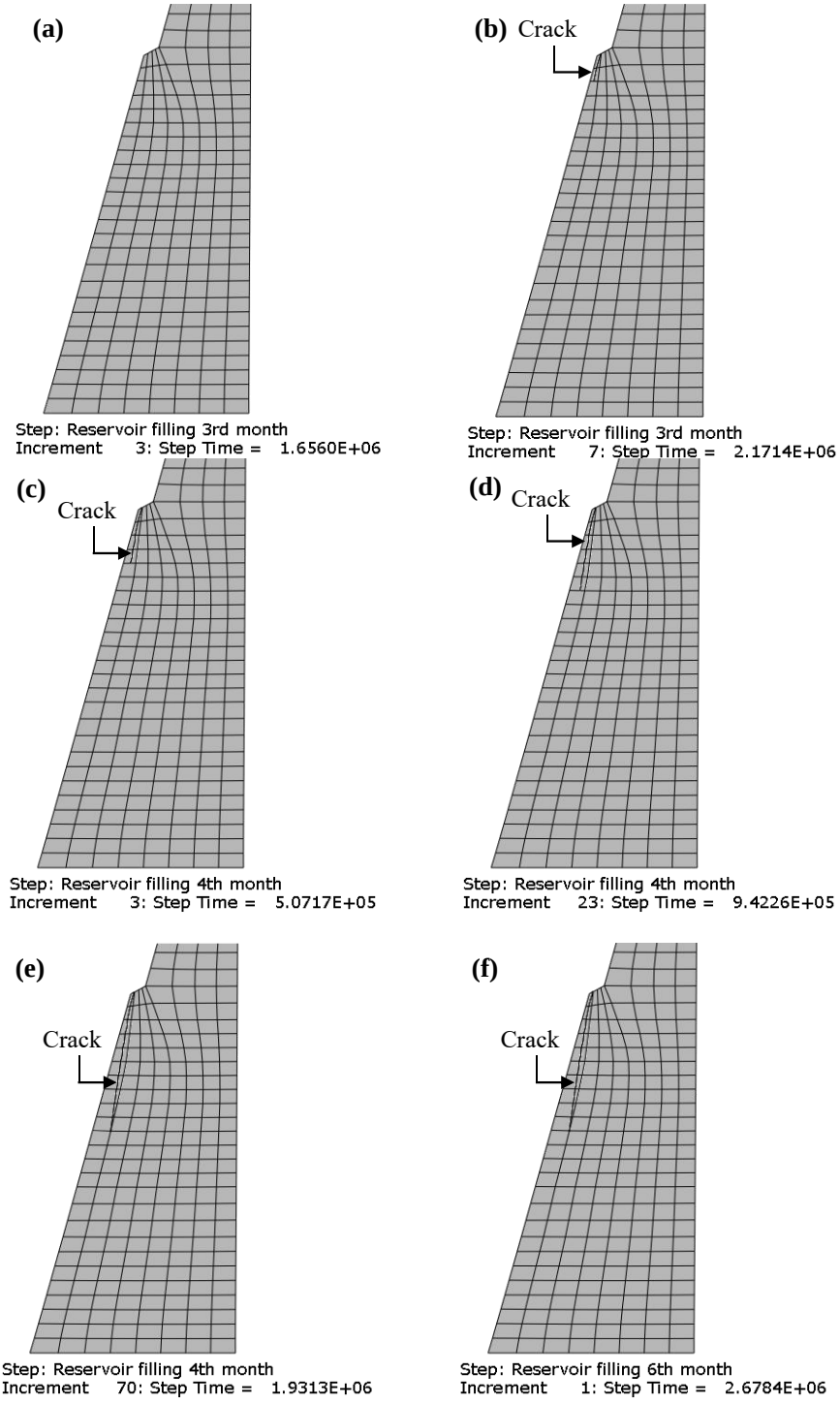

Figure 16. Evolution of crack in the core modelled using XFEM after (a) 2.6 months (b) 2.8 months (c) 3.2 months (d) 3.3 months (e) 3.7 months and (f) 6 months of reservoir filling

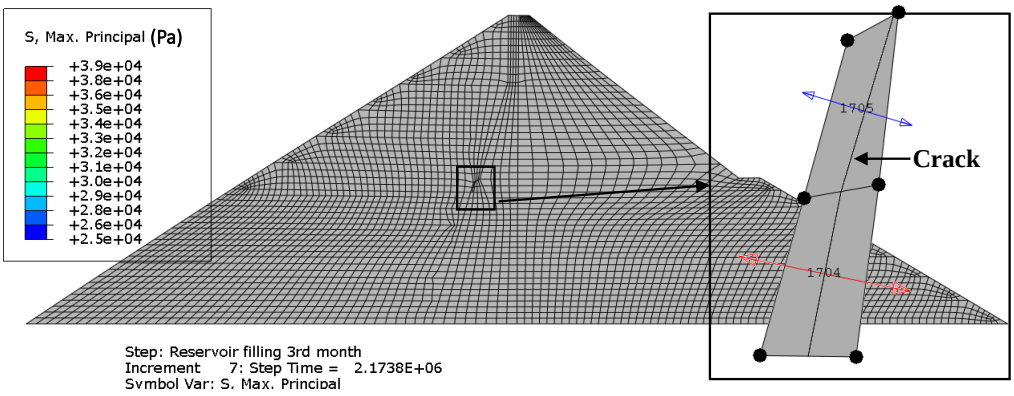

Figure 17. Maximum principal stress and crack initiation direction through the elements containing crack propagation pathway

Table 2. Characteristic properties of the dam materials used for various scenarios to assess the influence on hydraulic fracturing

Shell		Core			
		Cases			
ρ	2200 kg/m^3	I	ρ	2260 kg/m^3	k 1×10^{-10} m/s
E	50,000 kPa		E	20,000 kPa	
ν	0.3	II	ν	0.3	k 1×10^{-5} m/s
k	0.025 m/s	III	e	0.26	k 0.0225 m/s
e	0.6	IV	ρ	2260 kg/m^3	E 10,000 kPa
			ν	0.3	
		V	e	0.26	E 30,000 kPa
		VI	k	7×10^{-10} m/s	E 50,000 kPa
		VII	ρ	2260 kg/m^3	Maximum Reservoir level = 60 m
			E	20,000 kPa	
		VIII	ν	0.3	Maximum Reservoir level = 70 m
		IX	k	7×10^{-10} m/s	Maximum Reservoir level = 85 m
			e	0.26	

5.5.1 Influence of permeability of the core on hydraulic fracturing

In this section, influence of permeability of the dam core in inducing hydraulic fracturing is investigated. In reference to Case I, the permeability of core is adopted very low i.e. 1×10^{-10} m/s, which is close to the permeability value of Hyttejuvet dam core. In the subsequent cases, permeability is increased for the core material. In Case II, it is considered as 1×10^{-5} m/s, while in Case III, the permeability of the core is assumed to be same as that of the shell rock-fill material, i.e. 0.0225 m/s.

Figure 18 shows pore pressure development and crack growth in the dam for all three cases (Cases I, II and III) when the water level rises to its maximum value. The pore water pressure

577 contours in all three cases give an idea about the permeability taken for the core. It is observed
578 from the simulation results that in Case I, the crack initiates after 4 months from the reservoir
579 filling commencement while in Case II, it initiates after 5 months (the same can be noted in
580 Fig. 19). Figure 18 shows that the crack propagates to larger depth for Case-I than for Case-II,
581 both being illustrated for the 6^{th} month after commencement of impounding when water level
582 reaches the maximum. On the contrary, there is no initiation of crack in Case III, as in this
583 scenario, the presence of a highly permeable core facilitates the dissipation of pore pressure
584 rapidly. Hence, the developed tensile effective stress in the upstream face of the core is not, at
585 large, influential in crack initiation process. It can be concluded that increasing permeability,
586 or increasing the ease of flow through core, reduces the severity and likelihood of hydraulic
587 fracturing.
588
589 For all the three cases (Cases I, II and III), Fig. 19 shows the effective maximum principal
590 stress development on the upstream face of the core at the corresponding crack locations. It
591 shows that the compressive stress (negative) in the core keeps decreasing and as the pore
592 pressure builds up, the effective stresses transitions to become tensile (positive). When the
593 value reaches 20 kPa (the defined tensile strength of clay core), damage initiation starts and
594 cracks appear in the core. For Cases I and II, cracking is indicated by sudden decrease in the
595 tensile maximum principal stress. In Case III, there is no such stress drop as the tensile stress
596 does not reach the critical value and, hence, no crack initiates by the 6^{th} month of reservoir
597 impounding.
598
599 **5.5.2 Influence of the modulus of elasticity of the dam core**
600 According to previous studies (Kjærnsli and Torblaa 1968; Ng and Small 1999), hydraulic
601 fracturing occurs when total stress in the core is reduced by arching effect, which is further
602 affected by pore water pressure due to impounding. Increasing Young's modulus of the core
603 soil may reduce arching in the core and, subsequently, the likelihood of hydraulic fracture might
604 also decrease. In this section, a comparison of results of three cases (Cases IV, V and VI, as
605 shown in Table 2) has been reported based on increasing Young's modulus of core material
606 while keeping every other parameter of the dam same. For all the three cases as stated, Figure
607 20 shows the crack initiation and vertical stress contours within the dam body after 6 months
608 of impounding. It can be seen that stress arching is highest in Case IV and it decreases with the
609 increase the Young's modulus of core material. In case IV, the crack propagates to a very large
610 depth and nearly reaches the dam base; this phenomenon can cause severe leakage and failure

in the dam. As the Young's modulus of the core material is increased (Cases V and VI), the crack length observed to be not as severe as Case IV. It is understood that increasing Young's modulus of the core reduces the arching phenomenon, which, in turn, helps in reducing the likelihood of hydraulic fracturing in earth-fill zoned dams.

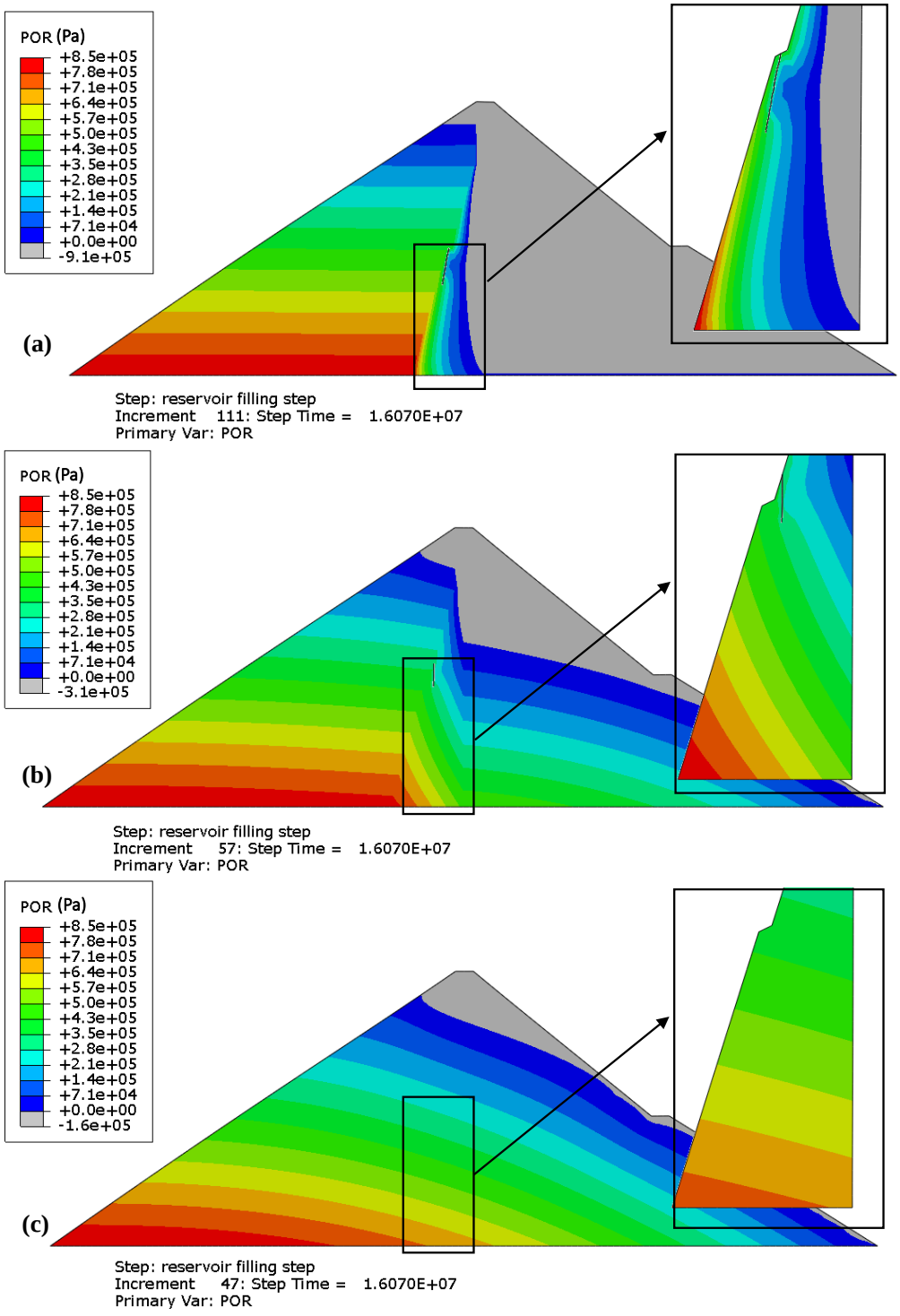

Figure 18. Pore-water pressure contours and corresponding initiation of fracture in the dam core for (a) Case I (b) Case II (c) Case III

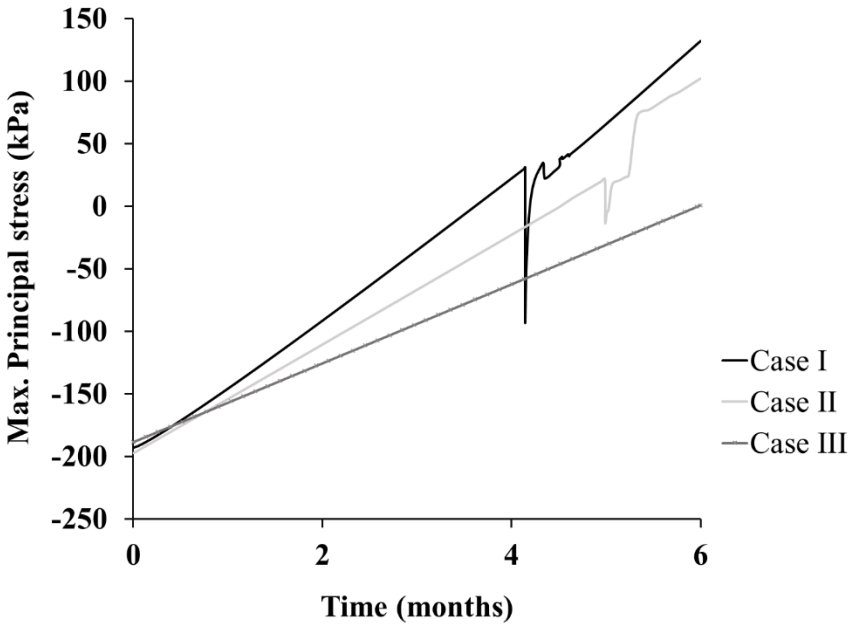

Figure 19. Effective maximum principal stress development on the upstream face of core at the location of the crack

5.5.3 Influence of reservoir water level on crack initiation at dam core

Three cases of varying reservoir water level (Cases VII, VIII and IX) are considered with the maximum water level at 60 m, 70 m, 85 m from the base (wherein the water level being linearly ramped up over a time period of 6 months). Figure 21 exhibits the pore pressure development and the status of the crack in the 6^{th} month of reservoir filling. It shows that increasing the water level induces larger crack length in the core in the 6^{th} month of reservoir filling. It is concluded that the severity of the induced hydraulic fracturing under high water levels is evidently more than in low water levels. As found by Wang (2014), the J-integral values increase with increasing water level, thereby concluding that the likelihood of occurrence of hydraulic fracturing is more in case of a higher water level. It is likely that optimizing the other factors that influence hydraulic fracturing and controlling the water level might help in totally avoiding hydraulic fracturing in earth and rock-fill dams. However, the effect of optimizing the parameters on the other engineering behaviour of the dam need to be ascertained, which is beyond the scope of the present study and can be attempted in future to develop a more comprehensive understanding of the multi-criteria failure of earth-rockfill dams.

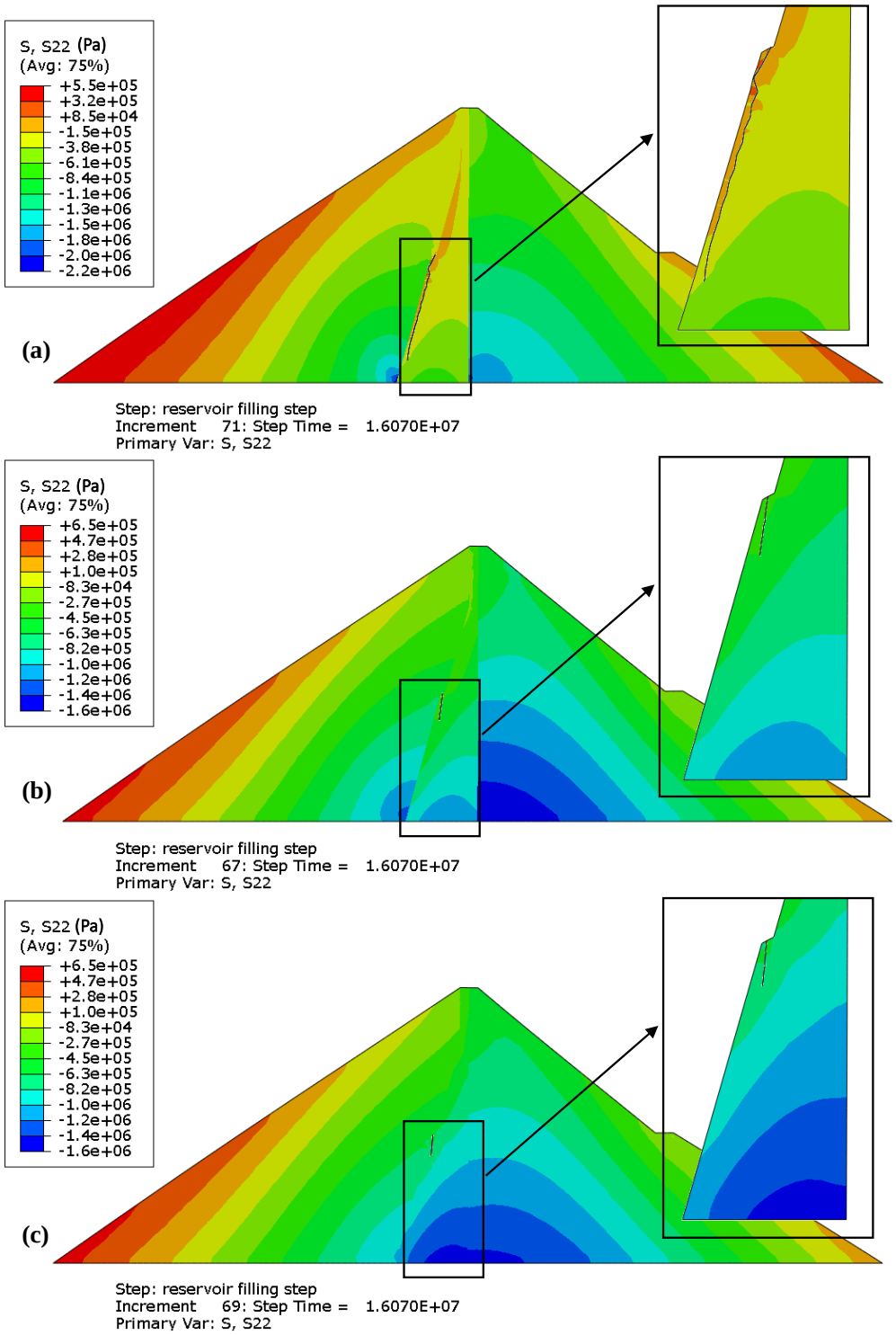

Figure 20. Effective vertical stress contour and corresponding initiation of fracture in the dam core for (a) Case IV (b) Case V (c) Case IV

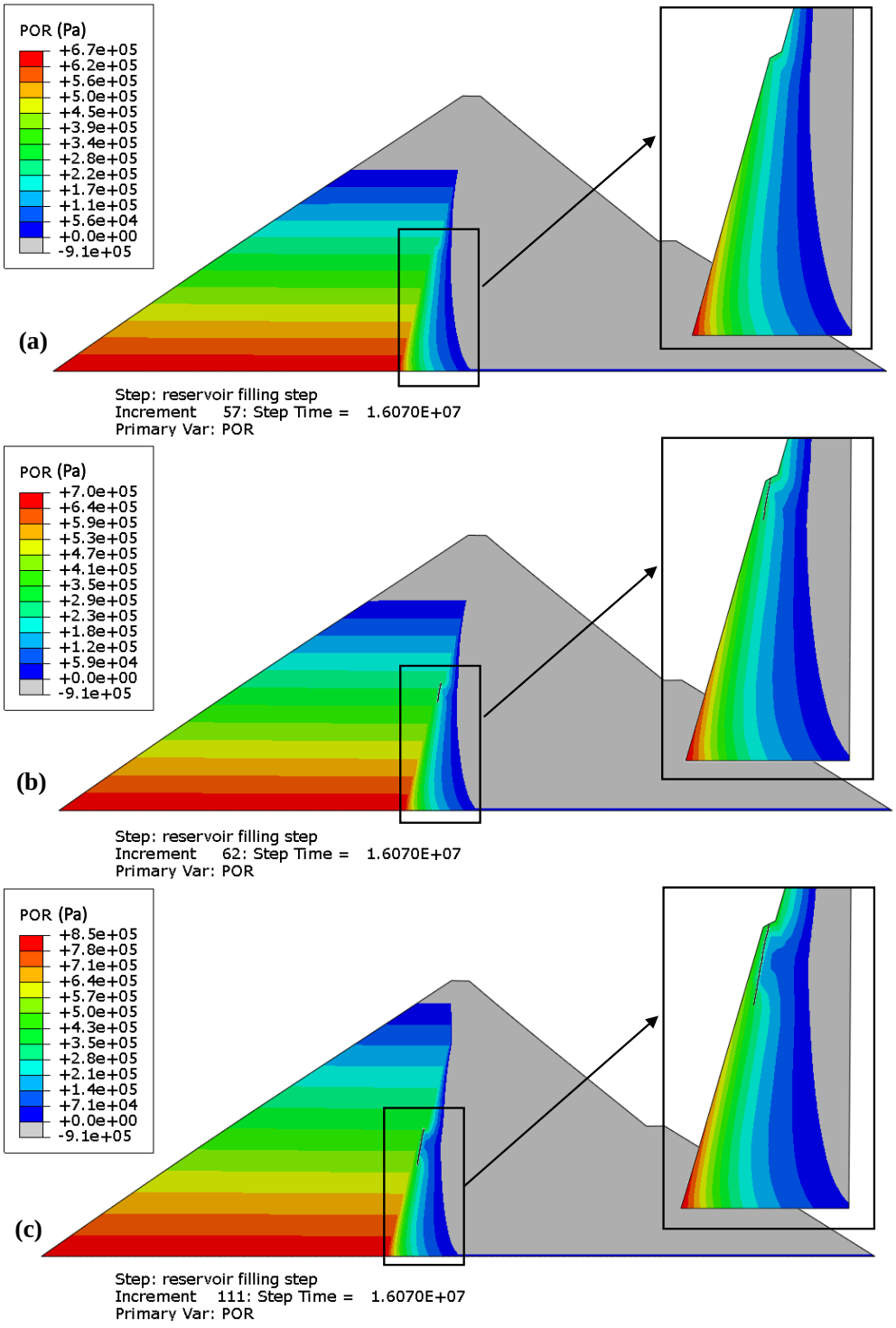

Figure 21. Pore-water pressure contours and corresponding initiation of fracture in the dam core for (a) Case VII (b) Case VIII (c) Case IX

6. Conclusions

Hydraulic fracturing in earth-rock fill dams is very complicated and important problem. A case study of hydraulic fracturing in Hyttejuvet dam using XFEM based cohesive segments

approach is presented in this manuscript. The behaviour of the dam during construction and filling of the reservoir is simulated using finite element method. The simulated results are supported by the good agreement between the computed and measured pore-water pressures that plays a crucial part in assessing the stress conditions within the dam. A significant stress arching phenomenon in the upstream face of the core is observed at the mid depth of the dam after the construction stage is completed, due to differential settlement between the rock-fill shells and the clay core. At the same depth, the hydraulic induced fracture initiates on the upstream face of core. Moreover, the timing of the fracture occurrence is in good agreement with the time when severe leakage was observed for the first time in the Hyttejuvet dam. The fracture propagates in a nearly vertical direction, orthogonal to the maximum tensile stress direction. Based on traction-separation criteria, the XFEM-based study helped to simulate hydraulic fracture initiation in the core and understand its evolution of fracturing in the core with time. Later, several factors affecting the behaviour of hydraulic fracturing has been investigated. It is concluded that increasing permeability of the core delays initiation of the fracture and crack grows up to a lesser depth within the core. Smaller crack may possess lesser threat to the dam structure. A lower permeable core allows significant growth of the crack, which, upon nearing the base of the dam, can cause devastating failure of the dam structure. It is comprehended that increasing the Young's modulus of the core soil would reduce arching phenomenon, thereby subsequently reducing the severity of the hydraulic fracture phenomenon. Increasing reservoir water level can induce larger crack in the core. Hence, it is important to properly design and plan the dam construction and reservoir operations in order to avoid such adverse scenarios of hydraulic fracturing or, alternatively, delay their formation and enhance the performance and longevity of the dam structure. It is concluded that all the said factors govern the behaviour of hydraulic fracturing in the earth-rock fill dam and optimizing these parameters would help the practicing engineers to reduce or avoid the likelihood of hydraulic fracturing.

Declaration of Competing Interests

The authors declare that there are no competing interests

Data Availability Statement

Data generated or analyzed during this study are available from the corresponding author upon reasonable request.

References

Adamo, N., Al-Ansari, N., Sissakian, V., Laue, J., and Knutsson, S. (2020). Dam safety and overtopping. *Journal of Earth Science and Geotechnical Engineering*, *10*, 41–78.

Angelakis, A.N., Baba, A., Valipour, M., Dietrich, J., Fallah-Mehdipour, E., Krasilnikoff, J., Bilgic, E., Passchier, C., Tzanakakis, V.A., Kumar, R., Min, Z., Dercas, N., and Ahmed, A.T. (2024). Water dams: From ancient to present times and into the future. *Water*, *16(13)*, 1889. https://doi.org/10.3390/w16131889

Barani, O. R., and Khoei, A. R. (2014). 3D modelling of cohesive crack growth in partially saturated porous media: a parametric study. *Engineering Fracture Mechanics*, *124-125,* 272-286. https://doi.org/10.1016/j.engfracmech.2014.04.016

Belytschko, T. and Black, T. (1999). Elastic crack growth in finite elements with minimal remeshing. *International Journal Numerical Methods in Engineering*, *45*, 601-620. https://doi.org/10.1002/(sici)1097-0207(19990620)45:5<601::aid nme598>3.0.co;2-s

Binnie, G M. (1983). Postscript to 'The collapse of the Dale Dyke dam in retrospect'. *Quarterly Journal of Engineering Geology and Hydrgeology*, *16*, 375- 358. https://doi.org/10.1144/gsl.qjeg.1983.016.04.11

Binnie, G.M. (1978). The collapse of the Dale Dyke dam in retrospect. *Quarterly Journal of Engineering Geology and Hydrogeology, 11*, 305 - 324. https://doi.org/10.1144/gsl.qjeg.1978.011.04.04

Bishop, A.W. (1959). The principle of effective stress. *Teknisk Ukeblad*, *106 (39)*, 859–863.

Chudnovsky, A., Saada, A., & Lesser, A. J. (1988). Micromechanisms of deformation in fracture of overconsolidated clays. *Canadian Geotechnical Journal*, *25*(2), 213-221. https://doi.org/10.1139/t88-025

Dascal, O. (1984). Peculiar behavior of the Manicouagan 3 dam's core. *Proceedings of the First International Conference on Case Histories in Geotechnical Engineering,* Missouri-Rolla, USA, 561-569.

Djarwadi, D., Suryolelono, K. B., Suhendro, B., and Hardiyatmo, H. C. (2017). Effect of clay core configuration of the rock fill dams against hydraulic fracturing. *Procedia Engineering*, *171*, 492-501. https://doi.org/10.1016/j.proeng.2017.01.361

Dounias, G. T., Potts, D. M., and Vaughan, P. R. (1996). Analysis of progressive failure and cracking in old British dams. *Geotechnique*, *46(4)*, 621-640. https://doi.org/10.1680/geot.1996.46.4.621

Fillunger, P. (1936). Erdbaumechanik? *Selbstverl. D. Verf.: Wien, Austria*.

717 Guerriero, V. and Mazzoli, S. (2021). Theory of effective stress in soil and rock and
718 implications for fracturing processes: A Review. *Geosciences*, *11*, 119.
719 https://doi.org/10.3390/geosciences11030119
720 Haeri, S. M. and Faghihi, D. (2008). Predicting hydraulic fracturing in Hyttejuvet
721 dam. *International Conference on Case Histories in Geotechnical Engineering,* Arlington,
722 Virginia. 40.
723 ICOLD. (1995). Dam failures: Statistical analysis. International Commission on Large Dams,
724 Bulletin 99.
725 Jaworski, G. W, Duncan, J. M., and Seed, H. B. (1981). Laboratory study of hydraulic
726 fracturing. *Journal of Geotechnical Engineering Division, ASCE, 107(6),* 713-732.
727 https://doi.org/10.1061/ajgeb6.0001147
728 Ji, E., Fu, Z., Chen, S., Zhu, J., Geng, Z. (2018). Numerical simulation of hydraulic fracturing
729 in earth and rockfill dam using extended finite element method. *Advances in Civil*
730 *Engineering*, 1-8. https://doi.org/10.1155/2018/1782686
731 Kjærnsli, B., and Torblaa, I. (1968). Leakage through horizontal cracks in the core of
732 Hyttejuvet dam. *Norwegian Geotechnical Institute Publication*, *80*, 39–47.
733 Komak Panah, A., and Yanagisawa, E. (1989). Laboratory studies on hydraulic fracturing
734 criteria in soil. *Soils and Foundations*. *29(4)*. 14-22.
735 https://doi.org/10.3208/sandf1972.29.4_14
736 Li, Q., Zhang, B. Y., Yu, Y. Z., and Wang, J. (2007). Numerical simulation of the process of
737 hydraulic fracturing in earth and rockfill dams. *Chinese Journal of Geotechnical*
738 *Engineering*, *29(2),* 212-217.
739 Lo, K. Y., and Kaniaru, K. (1990). Hydraulic Fracture in earth and rockfill dams. *Canadian*
740 *Geotechnical Journal, 27(4),* 496-506. https://doi.org/10.1139/t90-064
741 Lofquist, B. (1951). Earth pressure in a thin impervious core. *Transactions of the 4th*
742 *International Congress on Large Dams,* New Delhi, India*, 1,* 99-109.
743 Melenk, J.M. and Babusska, I. (1996). The partition of unity finite element method: Basic
744 theory and applications. *Computational Methods for Applied Mechanical Engineering*,
745 *139,* 289-314. https://doi.org/10.1016/s0045-7825(96)01087-0
746 Ng, A. K. L., and Small, J. C. (1999). A case study of hydraulic fracturing using finite element
747 methods. *Canadian Geotechnical Journal, 36(5),* 861-875. https://doi.org/10.1139/t99-
748 049

749 Ng, K. L. A., and Small, J. C. (1997). Behavior of joints and interfaces subjected to water
750 pressure. Computers and Geotechnics, *20(1)*, 71-93. https://doi.org/10.1016/S0266-
751 352X(96)00015-8
752 Nur, A. and Byerlee, J.D. (1971). An exact effective stress law for elastic deformation of rock
753 with fluids. *Journal of Geophysical Res*earch, *76*, 6414–6419.
754 https://doi.org/10.1029/jb076i026p06414
755 Oliver, J. (1995). Continuum modelling of strong discontinuities in solid mechanics using
756 damage models. *Computational Mechanics*, *17*, 49-61.
757 https://doi.org/10.1007/BF00356478
758 Penman, A. D. M., and Charles, J. A. (1981). Assessing the risk of hydraulic fracture in dam
759 cores. *Proceedings of the 10th International Conference on Soil Mechanics and*
760 *Foundation Engineering*, Stockholm, *1*, 457–462.
761 Rashid, M. (1998). The arbitrary local mesh refinement method: An alternative to remeshing
762 for crack propagation analysis. *Computational Methods for Applied Mechanical*
763 *Engineering*, *154*, 133-150. https://doi.org/10.1016/s0045-7825(97)00068-6
764 Secchi, S., and Schrefler, B. A. (2012). A method for 3-D hydraulic fracturing simulation.
765 *International Journal of Fracture*, *178(1-2),* 245-258. https://doi.org/10.1007/s10704-
766 012-9742-y
767 Seed, H. B., and Duncan, J. M. (1981). The Teton dam failure-A retrospective review.
768 *Proceedings of the 10th International Conference on Soil Mechanics and Foundation*
769 *Engineering,* Stockholm, Sweden, *4,* 214-238. https://doi.org/10.1016/s0266-
770 352x(96)00015-8
771 Sherard, J. L. (1973). Embankment dam cracking. *Embankment Dam Engineering;*
772 *Casagrande Volume*, Eds. R. C. Hirschfeld and S. J. Poulos, John Wiley, New York, 324-
773 328.
774 Sherard, J. L. (1986). Hydraulic fracturing in embankment dams. *Journal of the Geotechnical*
775 *Engineering Division*, *ASCE*, *112(GT10)*, 905–927. 10.1061/(ASCE)0733-
776 9410(1986)112:10(905)
777 SIMULIA User Assistance (2017). Dassault Systemes Simulia, Inc.
778 Skempton, A.W. (1960). Effective stress in soil, concrete and rocks. *International Conference*
779 *Pore Pressure and Suction in Soils.: London, UK*, 4–16.

780 Sukumar, N., Huang, Z.Y., Prévost, J.-H. and Suo, Z. (2004), Partition of unity enrichment for
781 bimaterial interface cracks. *International Journal Numerical Methods in Engineering*, 59,
782 1075-1102. https://doi.org/10.1002/nme.902
783 Talukdar, P. and Dey, A. (2019). Hydraulic failures of earthen dams and embankments.
784 *Innovative Infrastructure Solutions*, *4*, 1-20. https://dx.doi.org/10.1007/s41062-019-0229-
785 9
786 Talukdar, P. and Dey, A. (2021). Finite element analysis for identifying locations of cracking
787 and hydraulic fracturing in homogeneous earthen dams. *International Journal of*
788 *GeoEngineering, 12*, 1-26. https://doi.org/10.1186/s40703-020-00139-8
789 Tang, C.S., Pei, X.J., Wang, D.Y., Shi, B. and Li, J. (2015). Tensile strength of compacted
790 clayey soil. *Journal of Geotechnical and Geoenvironmental Engineering, ASCE*, *141*(4),
791 04014122. https://doi.org/10.1061/(asce)gt.1943-5606.0001267
792 Terzaghi, K. (1923). Die berechnung der durchlassigkeitsziffer des tones aus dem verlauf der
793 hidrodynamichen span nungserscheinungen akademie der wissenschaften in wien.
794 *Mathematish-Naturwissen-SchaftilicheKlasse: Mainz, Germany*, 125–138.
795 USBR (1976). Independent Panel to Review Cause of Teton Dam Failure. Report to U.S.
796 Department of the Interior and the State of Idaho on Failure of Teton Dam, U.S. Bureau of
797 Reclamation, Denver, CO.
798 USCOLD. (1988) Lessons from dam incidents, USA II. Committee on Dam Safety of the
799 United States Committee on Large Dams (USCOLD). American Society of Civil
800 Engineering, New York.
801 Vaughan, P.R., Kluth, D.J., Leonard, M.W., and Pradoura, H.H.M. (1970). Cracking and
802 erosion of the rolled clay core of Balderhead dam and the remedial works adopted for its
803 repairs. *Transactions of the 10th International Congress on Large Dams*, *ICOLD.*
804 Montréal, *1*, 73–93.
805 Vestad, H. (1976). Viddalsvatn dam: A history of leakages and investigations. *Transactions of*
806 *the 12th International Congress on Large Dams, ICOLD,* Mexico*, 2,* 369-390.
807 Wang, J.J. (2014). Hydraulic fracturing in earth-rock fill dams. John Wiley & Sons Singapore
808 Pte. Ltd. https://doi.org/10.1002/9781118725542
809 Wang, J.-J.; Zhu, J.-G., Mroueh, H and Chiu, C. (2007). Hydraulic fracturing of rock-fill dam.
810 *The International Journal of Multiphysics*, *1*, 199-219.
811 https://doi.org/10.1260/175095407781421595

812 Wiltshire, R.L. (2002). 100 years of embankment dam design and construction in the U.S.
813 Bureau of Reclamation. *Bureau of Reclamation History Symposium*, University of
814 Nevada-Las Vegas, Las Vegas, NV.
815 Zhu, J.G., and Wang, J. J. (2004). Investigation on arching action and hydraulic fracturing of
816 core rockfill dam. *Proceedings of the 4th International Conference on Dam Engineering*,
817 Rotterdam: Balkema, 1171-1180.